Photoluminescence Quantum Yield of Fluorescent Silicon Carbide Determined by an Integrating Sphere Setup

Wei, Yi; Ou, Haiyan

Published in:
ACS Omega

Link to article, DOI:
10.1021/acsomega.9b01753

Publication date:
2019

Document Version
Publisher's PDF, also known as Version of record

ACS OMEGA

Article

Cite This: ACS Omega 2019, 4, 15488−15495

http://pubs.acs.org/journal/acsodf

Photoluminescence Quantum Yield of Fluorescent Silicon Carbide Determined by an Integrating Sphere Setup

Yi Wei and Haiyan Ou*

Department of Photonics Engineering, Technical University of Denmark, DK-2800 Kgs. Lyngby, Denmark

ABSTRACT: The excitation-dependent photoluminescence quantum yield (PL-QY) of strong n-type nitrogen−boron codoped 6H fluorescent silicon carbide (f-SiC) at room temperature is experimentally determined for the first time. The PL-QY measurements are realized by an integrating sphere system based on a classical two-measurement approach. In particular, in accordance to the difference between our in-lab setup and the standard setup of the two-measurement approach, we have technically modified the experimental design, the data processing algorithm, and the estimation of relative uncertainty. The measured highest PL-QY of f-SiC samples is found to reach above 30%. We compare the PL-QYs at a certain excitation power of all f-SiC samples by considering their intrinsic defect densities. Finally, the evolution of the excitation power-dependent PL-QY of f-SiC is attributed to both band-to-band and impurity-assisted Auger recombination.

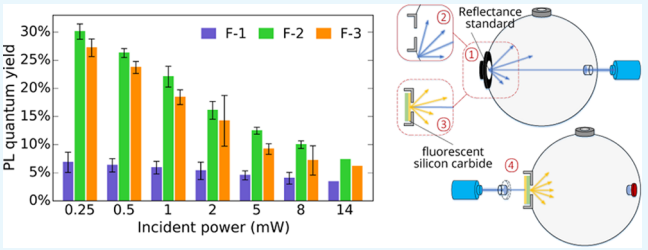

1. INTRODUCTION

White light-emitting diode (LED) light sources have been massively implemented in almost every aspect of industries and daily lives. Compared to traditional white light solutions, e.g., incandescent light bulbs, white LED light sources have several advantages. For instance, white LED light sources are more energy efficient, contain no mercury or other hazardous elements, and require no warm-up period. There are three configurations of white LED light sources. The first is the so-called tricolor configuration that consists of a red, a green, and a blue LED; however, the color mixing corresponding to this design is not very smooth. The second is the most commercialized type that is made of a blue LED covered by yellow phosphors. As blue LEDs and yellow phosphors are very efficient, this type of white LED can induce high luminescent efficiency. However, as the typical yellow phosphor is made of cerium-doped yttrium aluminum garnet, i.e., (YAG):Ce,[1] its degradation issue would cause the white LED light source to have a low color rendering index (CRI). Moreover, the cost and supply issues regarding the rare earth elements in yellow phosphors, e.g., Ce in (YAG):Ce, should be also concerned. The last configuration is composed of a near-ultraviolet (NUV) LED covered by red/green/blue phosphors. Note that this type of white LED light source can induce high CRI, but the efficiency of the red phosphor is quite low. Fortunately, a new type of inorganic phosphor grown by Kamiyama et al.,[2] i.e., the donor and acceptor codoped fluorescent silicon carbide (f-SiC), which contains no rare earth elements and has no degradation issues, is anticipated to realize NUV excitation-based white light emission that could reach out an optimized tradeoff between the luminous efficacy and CRI. By getting heavily nitrogen−boron (N−B) codoped, f-SiC can be applied as a passive wavelength conversion medium, where strong orange-yellowish light emission with large full width at half-maximum (FWHM) can be generated by optically pumping f-SiC via a NUV light source, e.g., a nitride-based NUV LED chip. It is also worth noting that SiC is regarded as a better platform for the integration of a nitride-based NUV LED chip compared to the prevalent sapphire substrate. In addition, another type of f-SiC that is nitrogen−aluminum (N−Al) codoped is anticipated to emit blue-green light by NUV light source pumping.[3] It has been proposed[4,5] that a new type of white LED light source with high CRI can be achieved by growing the stacking structure that contains a nitride-based NUV LED chip, a N−B as well as a N−Al codoped f-SiC layer as shown in Figure 1.

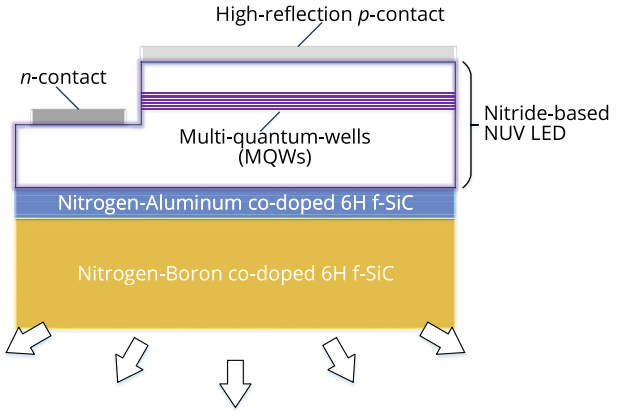

Figure 1. Schematic diagram of the stacking structure of a white LED based on N−B and N−Al codoped f-SiC thin films.

Received: June 13, 2019
Accepted: August 27, 2019
Published: September 11, 2019

DOI: 10.1021/acsomega.9b01753
ACS Omega 2019, 4, 15488−15495

Since N−Al codoped SiC does not show photoluminescence (PL) at room temperature (RT), in the scope of this research, f-SiC usually refers to N−B codoped SiC. Two methods have been proposed to enhance the intensities of the donor−acceptor pair (DAP) recombination events in f-SiC, i.e., increase the density of DAP and the sample thickness. Luckily, the above-mentioned two methods have been successfully implemented in the epilayer growth of f-SiC, thanks to the advent of fast sublimation growth process (FSGP) method developed by Syväjärvi et al.,[6] which makes the current f-SiC have N−B codoping beyond 10^{18} cm^{-3}. In addition, with the FSGP method, it is also easy to achieve sufficient epilayer thickness since the growth rate of FSGP can be up to 200 $\mu m \cdot h^{-1}$.[77] Furthermore, the densities of the 1-D (i.e., micropipe), two-dimensional (i.e., stacking fault), and three-dimensional[8] (i.e., polytype switch, carbon inclusion, and silicon droplet) defects in f-SiC have been drastically decreased to the negligible levels[6,9] by applying the FSGP method for the growth of f-SiC epilayers. Meanwhile, the source SiC material for FSGP is prepared via the modified physical vapor transport technique developed by Wellmann et al.,[8,10,11] where the stable nitrogen doping and low dislocation densities in the source SiC material have been realized.

As knowing the photoluminescence quantum yield (PL-QY) of f-SiC, i.e., the ratio of the emitted photons to the absorbed photons of the f-SiC thin film, is of great importance for the evaluation of the upper limit of the external quantum efficiency of the entire white LED device shown in Figure 1. In this research, we demonstrate the experimental methodology regarding the determination of the PL-QY on n-type f-SiC samples. Note that only n-type f-SiC shows strong emission at RT where the reason regarding the distinctive luminescent behaviors of n- and p-type f-SiCs has been investigated before.[12] In addition, we also give the explanation for the physical mechanism corresponding to the incident power-dependent PL-QY of f-SiC.

There are two categories for the PL-QY measurement on a fluorescent material, i.e., the relative and absolute techniques.[13] For the relative technique, a standard f-SiC sample is needed whose PL-QY is already known. It is required that the standard f-SiC should have similar excitation, absorption, and emission properties to those of the sample to be measured. Since it is difficult to fully duplicate the experimental conditions in which the reference spectra of the standard f-SiC are measured in our lab, in this research, we adopt the absolute techniques for the PL-QY measurements. As f-SiC is a solid thin-film sample with high refractive index, the issues of anisotropic light emission and wave-guiding effects[14] could greatly affect the accuracy of the results of PL-QY measurement. A direct solution might be mapping the light emission to the solid angle distribution where the ratio of the detected PL emission to the whole PL emission can be determined by referring the experimental conditions related to PL excitation/detection. However, this solution is quite cumbersome and not so viable where heavy workload is required and the interval of the solid angle needs to be carefully chosen. On the other hand, integrating sphere has been recognized as the standard equipment for measuring the PL-QY of solid thin films.[15,16] By implementing integrating sphere into PL-QY measurements, all of the reflected and emitted light can be collected where the concern regarding the angular dependence of the PL emission is no longer needed. Therefore, the integrating sphere-based measurement system has been widely applied in the determination of PL-QY of solid thin films.[14,16−19] There are two types of methodologies based on the integrating sphere system for absolute determination of PL-QY,[20] i.e., three-measurement[14,17,21] and two-measurement[18,22,23] approaches. In fact, the two-measurement approach proposed by Johnson et al.[18] was derived from the three-measurement one developed by de Mello et al.[14] Afterward, Leyre et al.[20] have theoretically proved that the values of the PL-QY determined by these two approaches are identical. In this research, by applying an integrating sphere system, we developed the experimental procedure regarding the determination of f-SiC's PL-QY derived from the classical two-measurement approach. The reason behind the differences in the PL-QY of all f-SiC samples under the same excitation power was investigated. Additionally, we also tried to elaborate the trend of PL-QY against the changed excitation power regarding the certain f-SiC sample as well.

2. RESULTS AND DISCUSSION

2.1. PL-QY of Strong n-Type f-SiC. In this research, three N−B codoped strong n-type f-SiC samples, i.e., F-1/2/3, were employed in PL-QY measurements, where the basic parameters for these three f-SiC samples are summarized in Table 1.

Table 1. Parameters for the Three f-SiC Samples at RT, where d_{epi}/d_{sub} Refers to the Substrate/Epilayer Thickness[a]

sample	F-1	F-2	F-3
d_{sub} (μm)		250	
d_{epi} (μm)	45	150	250
N_d ($\times 10^{18}$ cm^{-3})	9.2	2.85	2.55
N_a ($\times 10^{18}$ cm^{-3})	5.2	1.10	1.50
N_d/N_a	1.77	2.60	1.70

[a] N_d and N_a are measured by time-of-flight secondary-ion mass spectroscopy.

By applying the FSGP method,[6] the epilayers of the f-SiC samples were grown on the (0001) plane of the commercial 6H-SiC substrates (SiCrystal GmbH) with low off-axis (orientation $\langle 11\bar{2}0 \rangle \pm 1.4°$) at 1725 °C. Note that sample F-1 and samples F-2/3 were grown in two separate batches.

For the experimental design, data processing algorithm, and the estimation of uncertainty regarding the PL-QY determination of f-SiC samples, refer to Section 4.1. The PL-QYs of each sample were excited under seven different incident beam powers, i.e., 0.25, 0.5, 1, 2, 5, 8, and 14 mW, to study the power dependency of f-SiC's PL-QY. Note that the PL-QYs for all three samples were measured twice with the incident beam power from 0.25 to 8 mW, where the measurements corresponding to the beam incidence of 14 mW were only launched for once due to the unstable fiber-coupled maximum output power of the laser source. The uncertainties of the measured PL-QYs for each sample with specific incident power have been estimated using eq 11, where all of the U_{PL} values together with the respective mean values of η_{PL} are presented in Figure 2.

From Figure 2, it is clearly seen that the PL-QYs of F-1 under all incident powers are lower than those of F-2/3. On the other hand, we also measured the time-resolved photoluminescence (TRPL) of these three samples, where different numbers of spots were characterized on different samples (F-1, nine; F-2/3, three). The TRPL measurement results are summarized in Figure 3, and the related experimental details are given in Section 4.2. Compared to F-1, F-2/3 have slower

DOI: 10.1021/acsomega.9b01753
ACS Omega 2019, 4, 15488−15495

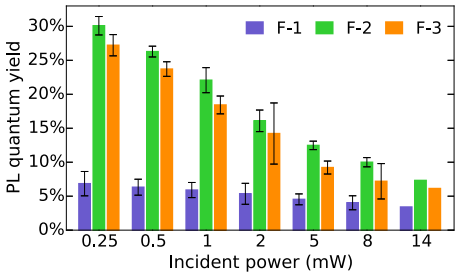

Figure 2. Averaged PL-QYs of samples F-1/2/3. The error bars indicate the relative uncertainties (U_{PL}) of the PL-QY measurements that were calculated using eq 11.

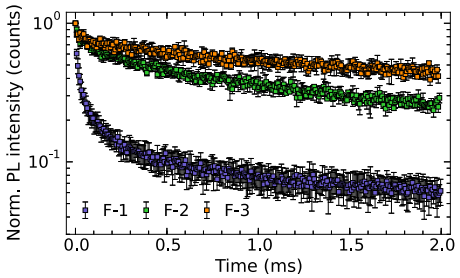

Figure 3. Normalized TRPL decays recorded via time-correlated single-photon counting (TCSPC) histograms for samples F-1/2/3. Each error bar indicates the standard deviation normalized by the corresponding photon count at a certain time point.

PL decay at the initial stage. This indicates that the lifetimes, τ, corresponding to the decay channels of E_1/E_2 centers, which have been confirmed[24] as the dominating intrinsic defects in 6H f-SiC, in F-2/3 are longer. Assuming that these three samples have the identical hole capture cross sections (σ_h) corresponding to the E_1/E_2 centers, the densities of E_1/E_2 centers can be estimated by $N = (\sigma_h\langle\nu_{th,h}\rangle\tau)^{-1}$, where $\langle\nu_{th,h}\rangle$ refers to the mean thermal velocity of nonequilibrium holes. Hence, it is clear to see that the densities of E_1/E_2 centers are higher in sample F-1 compared to those of F-2/3, which is considered as the one of the major causes regarding the gap in PL-QYs of F-1 and F-2/3.

In addition, regarding the NUV beam excitation on the front sides of the three samples, by considering the effective penetration depth, Z_{eff}, as the depth where the intensity of the incident beam has just decreased to the midpoint between the original intensity and the attenuated intensity at the bottom of the thin film, one can build up the relation $[I_0 + I_0\exp(-\alpha d)]/2 = I_0\exp(-\alpha Z_{eff})$; then, we have the expression of Z_{eff} as shown in eq 1. Note that d refers to the sample thickness that should be equal to the sum of d_{epi} and d_{sub}; in our case, the absorption coefficient, α, is about 400 cm^{-1} at 375 nm[25] with $E \perp c$ configuration and I_0 is the incident NUV beam intensity.

$$Z_{eff} = \frac{1}{\alpha}\ln\left[\frac{2}{1 + \exp(-\alpha d)}\right] \quad (1)$$

Interestingly, by applying eq 1 for these three samples, it was found that they share almost the identical value of Z_{eff}, which is around 17.33 μm, due to their very large values of d. As a result, it is believed that[26] samples F-1/2/3 have an identical injection level g ($cm^{-3}\cdot s^{-1}$) since their effective penetration depths are equal. Hence, with the same amount of injected photons for the three samples, one half of the photons actually get absorbed within the depth of 0 to Z_{eff}. Meanwhile, it is considered that almost all of the other half of photons are absorbed within the depth of Z_{eff} of 45 μm, which means the proportions of the photons being absorbed by the substrates for all three samples can be negligible. Hence, it is believed that with the identical effective penetration depth, Z_{eff}, as well as sufficient epilayer thickness, d_{epi}, for all three samples, the differences regarding their PL-QYs are not correlated to their different sample thicknesses. In addition, the reason why sample F-2 has slightly higher PL-QY compared to that of F-3 is still not clear. By considering the emission of each f-SiC sample, which is mainly contributed by the upper part of the respective epilayer, i.e., from the epilayer surface to Z_{eff}, as a point source, the proportion of the emission from the edges of each f-SiC sample is proportional to its sample thickness, d.[27] Therefore, the PL-QY of F-3 might be more underestimated due to its lesser sample thickness compared to that of F-2, which causes the measured PL-QY of F-3 to be lower than that of F-2. Another reason can be derived from the doping conditions of F-2/3. Regarding the summarized N_d/N_a in Table 1, we can see that only the N_d/N_a for F-2 is higher than 2 compared to that for F-1/3, where the higher proportion of n-type dopant in F-2 might further compensate the non-radiative behavior regarding the shallow N-induced donors.[28]

2.2. Auger Recombination in f-SiC. In addition, an obvious tendency can be observed from Figure 2 that the PL-QY of the n-type 6H f-SiC sample increases with the decrease in incident power. We believe that this phenomenon is caused by the enhanced Auger recombination in the f-SiC sample when the incident power density on the sample is increased.[29] In particular, it has been observed that[30] a fast decay component emerges during free carrier absorption (FCA) measurement on SiC at elevated injection levels, where this fast decay channel is attributed to band-to-band Auger recombination. Moreover, it is well known that the rate of Auger recombination is proportional to the cube[31] of the total carrier densities, i.e., $n_0 + \Delta n$, where Δn refers to the density of nonequilibrium carriers. As the focused incident beam spot on the sample port of the integrating sphere has the diameter of 3 mm, the calculated injection level on f-SiC samples corresponding to the range of the incident beam power, i.e., 250 μW to 14 mW, is from 1.33×10^{18} to 7.47×10^{19} $cm^{-3}\cdot s^{-1}$. Therefore the change of the Auger recombination rate is expected to be more than 1 order of magnitude in the PL-QY measurements. On the other hand, it is worth mentioning that the phononless $e^- - e^- - h^+$ related Auger recombination becomes prominent for strong n-type SiC,[32] where the shallow donors could be involved in an impurity-assisted Auger process. This could also be one of the major causes regarding why the PL-QY of F-1 is far lower as its N_d is much higher compared to that of F-2/3. Future work about the characterization of the carrier lifetimes in f-SiC at high injection levels by the experimental technique like time-resolved FCA[33−35] is needed to study how the PL-QY is degraded by Auger recombination and its carrier dynamics.

3. CONCLUSIONS

In this research, we have designed the experimental scheme related to the absolute PL-QY determination on f-SiC samples, where the measurement methodology was based on a modified two-measurement approach using an integrating sphere. The algorithm corresponding to the data processing and the uncertainty estimation of PL-QY experimental results were also

DOI: 10.1021/acsomega.9b01753
ACS Omega 2019, 4, 15488−15495

developed. This newly developed PL-QY determination procedure is suitable for measuring the PL-QY of the thin-film sample with very weak emission (compared to the intensity of the excitation beam), e.g., indirect band gap thin films. The excitation power-dependent PL-QY of the three n-type 6H f-SiC samples, i.e., F-1/2/3, have been measured. By combining the PL-QY and TRPL measurement results for these three f-SiC samples, it was revealed that the PL-QY of f-SiC can be influenced by its densities of E_1/E_2 centers, which are the major nonradiative centers in f-SiC. A clear tendency where the PL-QY of f-SiC sample increases with the decreasing incident power indicates strong Auger recombination in f-SiC at high injection levels. It is believed that the Auger recombination in strong n-type f-SiC can be enhanced by the increased density of either injected carriers or the n-type dopant, where the latter could induce impurity-assisted phononless e^-−e^-−h^+ type of Auger recombination related to shallow donors.

4. EXPERIMENTAL SECTION

4.1. PL-QY Determination. For the determination of PL-QY of f-SiC samples, an integrating sphere (OL 700-71, Gooch & Housego) with a diameter of 6 in., a continuous diode NUV laser with λ = 375 nm (LBX-375 HPE), and an optical spectrometer (CAS 140B, Instrument Systems GmbH) were employed. Note that the integrating sphere applied in this measurement has only one sample port on the edge of the integrating sphere. This makes the measurement condition different from that of the classical two-measurement approach where the sample is placed at the center of the integrating sphere.[20] Therefore, the classical two-measurement approach has to be modified to match our measurement condition. In addition, the related algorithm of experimental data processing and the evaluation of relative uncertainty regarding the estimation of PL-QY have to be redeveloped as well. The important symbols and corresponding descriptions applied in this experiment are summarized in Table 2.

4.1.1. Measurement System Design. As a matter of fact, for the classical two-measurement approach,[20] the PL emission from a fluorescent sample collected by an integrating sphere, where the sample is placed at the center of the sphere, can be divided into four aspects depending on the conditions related to excitation and detection. The PL emission is considered to be collected under four conditions, i.e., front excitation−front detection (FEFD), front excitation−back detection (FEBD), back excitation−front detection (BEFD), and back excitation−back detection (BEBD), as shown in Figure 4.

Note that during the PL-QY determination on f-SiC samples, it was found that the luminescence intensities regarding the two configurations with back excitation, i.e., PL_{BEBD} and PL_{BEFD}, are almost undetectable. This is because that the excitation beam has been largely attenuated when it reaches to the interface between the f-SiC epilayer and the 6H-SiC substrate from backside. In addition, as the emission from the edges of each f-SiC sample is originated from the leaky modes[36] corresponding to the planar waveguide cavity, where the leaky modes are evanescent in the air, the detected intensities regarding this type of emission can be treated as negligible. To sum up, there are altogether four types of luminescence spectra required, i.e., the spectra of the original and attenuated excitation beams without/with the sample presented inside the integrating sphere (their integrated luminescent intensities are denoted L_a and L_c, respectively),

Table 2. Part of the Symbols and Related Descriptions Applied in the Experimental of PL-QY Determination on f-SiC Samples

symbol	description
	(↓ Integrated emission intensities of the source beam)
L_a	original, without sample excitation
L_c	attenuated, with sample excitation
	(↓ Integrated PL intensities of the f-SiC sample)
P_c	overall
PL_{FEFD}	front excited−front detected
PL_{FEBD}	front excited−back detected
PL_{BEFD}	back excited−front detected
PL_{BEBD}	back excited−back detected
	(↓ Measured spectrum, range: 350−784 nm, with OD filter)
$I_{SRC,W}(\lambda)$	source beam
$I_{FEFD,W,dir}(\lambda)$	front excited−front detected PL of f-SiC
$I_{FEBD}(\lambda)$	front excited−back detected PL of f-SiC
	(↓ Measured spectrum, range: 390−784 nm, without OD filter)
$I_{SRC,N}(\lambda)$	source beam
$I_{FEFD,N,ind}(\lambda)$	tail part of the source beam existing in $I_{FEFD,N,dir}(\lambda)$
$I_{FEFD,N,dir}(\lambda)$	front excited−front detected PL of f-SiC
SCR	scaling factor
SG filter	Savitzky−Golay filter
T_{SUB}	transmittance of the f-SiC substrate

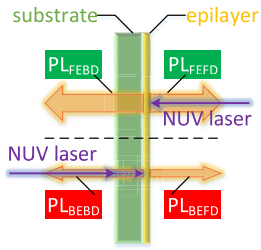

Figure 4. Four configurations related to the PL emission from a f-SiC sample (i.e., f-SiC epilayer + 6H-SiC substrate). As for the subscripts of the names of PL signals, "F", "B", "E", and "D" represent front, back, excitation, and detection, respectively, where the front side of the f-SiC sample refers to the side of epilayer.

and PL_{FEFD}/PL_{FEBD} (the total integrated PL intensity from the sample is denoted P_c), to extract sample's PL-QY. Note that the aforementioned notations, i.e., L_a | L_b | L_c are adopted from de Mello et al.[14] Figure 5 shows the experimental design based on the 6 in. diameter integrating sphere OL 700-71 for the PL-QY determination on f-SiC samples in this research. It is worth mentioning that the incident beam power was calibrated by measuring it at the sample port with a power meter (energy meter PM100D with a silicon detector S130VC, Thorlabs, Inc.) before steps 1 and 4 to ensure the same incident power for the reflectance/transmittance fiber optic probe (FOP). The spectra recorded through the four steps of the PL-QY measurement are summarized in Table 3 with specifications. Taking the measurement results of sample F-1 with the incident power of 5 mW based on the experimental setup shown in Figure 5 as an example, the measured spectra defined in Table 3 are shown in Figure 6.

4.1.2. Data Processing Algorithm. In step 1, a certified Reflectance Standard (Refl-Std), which is made of pressed poly(tetrafluoroethylene) powder packed in a 2 in. diameter holder, was installed on the sample port for measuring the original spectra of the excitation beam, where the Refl-Std was

DOI: 10.1021/acsomega.9b01753
ACS Omega 2019, 4, 15488−15495

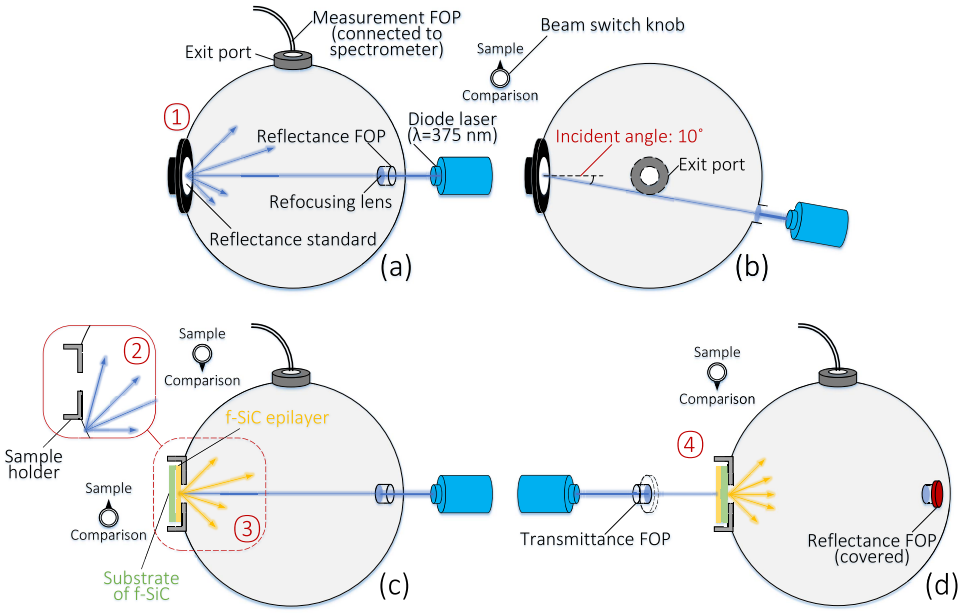

Figure 5. Diagram of the modified experimental procedure of PL-QY measurements on f-SiC samples. (a) Step 1, measurement of L_a. (b) Top view of the integrating sphere during step 1. (c) Steps 2 and 3, measurement of L_c and PL_{FEFD}, where the beam was directed toward the vicinity of the sample port (i.e., comparison mode) for step 2. (d) Step 4, measurement of PL_{FEBD}.

Table 3. Procedure of Recording One Set of Spectra for the PL-QY Determination for the f-SiC Sample Using the Experimental Configuration Shown in Figure 5[a]

step no.	spectrum name	toward sample port	range of λ	connected FOP	beam switch
1	$I_{SRC,W}(\lambda)$	Refl-Std	wide	Refl.	Samp.
	$I_{SRC,N}(\lambda)$	Refl-Std	narrow	Refl.	Samp.
2	$I_{FEFD,N,ind}(\lambda)$	sample holder	narrow	Refl.	Comp.
3	$I_{FEFD,N,dir}(\lambda)$	f-SiC front	narrow	Refl.	Samp.
	$I_{FEFD,W,dir}(\lambda)$	f-SiC front	wide	Refl.	Samp.
4	$I_{FEBD}(\lambda)$	f-SiC front	wide	Tran.	Comp.

[a]Note that the "wide" and "narrow" modes under "range of λ" refer to 350−784 and 390−784 nm, respectively. "W" and "N" in subscripts of spectrum name are also related to the wide and narrow modes, respectively. "ind" and "dir" refer to the indirect and direct incidence of the excitation beam on the sample port with the sample holder mounted, which correspond to the comparison mode (comp.) and sample mode (samp.), respectively. In addition, $I_{SRC,W}(\lambda)$ | $I_{FEFD,W}(\lambda)$ were recorded using the same parameter setting, i.e., integration time, time of collection, and choosing OD filter or not, and so were $I_{SRC,N}(\lambda)$ | $I_{FEFD,N,ind}(\lambda)$ | $I_{FEFD,N,dir}(\lambda)$.

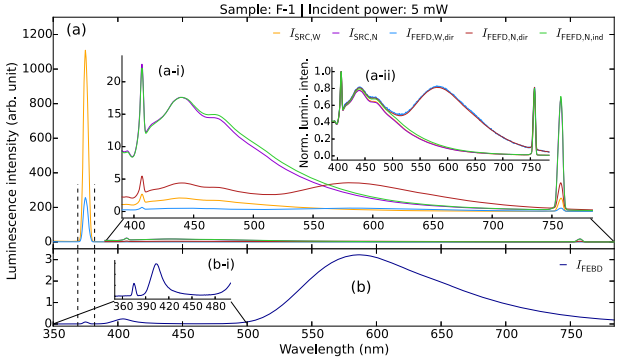

Figure 6. One set of spectra for the extraction of the PL-QY at certain incident power (here taking the measurement results corresponding to sample F-1 at an incident power of 5 mW as an example). According to the procedure of PL-QY measurement summarized in Table 3, the spectra recorded in steps 1−3 are presented in (a), whereas the spectrum recorded in step 4 is presented in (b). Note that the zoomed spectra in (a) at the predefined narrow wavelength range, i.e., 390−784 nm, are presented in inset (a-i), whereas the respective normalized spectra are shown in inset (a-ii). Inset (b-i) shows the zoomed spectrum of I_{FEBD} at the 350−500 nm range.

used for preventing light leakage through the sample port. $I_{SRC,W}$ and $I_{SRC,N}$ are the two spectra related to the original source beam measured in different wavelength ranges, i.e., the wide mode (350−784 nm) and the narrow mode (390−784 nm), respectively. Normally, an optical density filter (OD filter) was used when measuring $I_{SRC,W}$ to prevent the absolute intensity of its main peak centered at 375 nm from exceeding the upper detection limit of the optical spectrometer. Here, we got the expression of the integrated intensity of the original excitation spectrum (L_a) shown in eq 2, where Refl-Std(λ) refers to the reflectance spectrum of the Refl-Std.

$$L_a = \int_{369nm}^{382nm} \frac{I_{SRC,W}(\lambda)}{\text{Refl-Std}(\lambda)} d\lambda \quad (2)$$

In panel (a) of Figure 6, the spectrum of $I_{FEFD,W,dir}$, which includes the spectrum of PL_{FEFD}, was also measured with the OD filter. From the normalized spectrum of $I_{FEFD,W,dir}$ shown in inset (a-ii) of Figure 6, we can see that by adding the OD filter the line shape of $I_{FEFD,W,dir}$ is affected by ambient noise due to its weak intensity. In addition, the spectrum presented in panel (b) of Figure 6, i.e., I_{FEBD}, which reflects the information of the line shapes related to PL_{FEBD}, was measured without the OD filter. It can be expected that if the OD filter was added during the measurements of I_{FEBD}, the related spectrum would be also affected by the ambient noise. As a consequence, we decided to measure the spectra that were used for extracting the PL emission spectra without adding the OD filter. To establish the correlation between the spectra measured with/without the OD filter, a scaling ratio (SCR)

DOI: 10.1021/acsomega.9b01753
ACS Omega 2019, 4, 15488−15495

expressed by eq 3 is needed. Note that the values of both components in eq 3 should be similar since the degree of attenuation resulted by the OD filter is a constant. Accordingly, the extracted PL spectra related to the FEFD/FEBD configuration have to be scaled down by a factor of SCR to calculate PL-QY. The modified expression for PL-QY is shown in eq 4 where the value of PL-QY is denoted by η_{PL} and $P_{c,FEBD}/P_{c,FEFD}$ refers to the integrated PL intensity of $PL_{FEFD}(\lambda)/PL_{FEBD}(\lambda)$, respectively.

$$SCR = \frac{1}{2} \times \frac{\int_{390nm}^{784nm} I_{SRC,W}(\lambda)d\lambda}{\int_{390nm}^{784nm} I_{SRC,N}(\lambda)d\lambda} + \frac{1}{2} \times \frac{\int_{390nm}^{784nm} I_{FEFD,W,dir}(\lambda)d\lambda}{\int_{390nm}^{784nm} I_{FEFD,N,dir}(\lambda)d\lambda} \quad (3)$$

$$\eta_{PL} = \frac{1}{SCR} \times \frac{P_{c,FEBD} + P_{c,FEFD}}{L_a - L_c} = \frac{1}{SCR} \times \frac{\int_{450nm}^{784nm} PL_{FEBD}(\lambda) + PL_{FEFD}(\lambda)d\lambda}{L_a - L_c} \quad (4)$$

From the inset (a-ii) of Figure 6, we can see that the line shapes of the spectra of the excitation beam measured with/without the OD filter (i.e., $I_{SRC,W}/I_{SRC,N}$, respectively) are identical and so are the two spectra of the PL emission with FEFD configuration ($I_{FEFD,W,dir}$ and $I_{FEFD,N,dir}$). It is confirmed that spectra are scaled down by the OD filter regardless of the wavelength; hence, it is reasonable to apply SCR for PL-QY calculation. The upper limit of the detectable wavelength (i.e., 784 nm), which is also shown in eqs 3 and 4, is actually caused by the limitation of the optical spectrometer. It is believed that the PL intensity of the f-SiC samples with wavelength shorter than the lower limits of the integrals in eq 4 (i.e., 450 nm) can be negligible. In the inset (a-i) of Figure 6, it is clearly seen that the spectrum of the excitation beam has a tail part that consists of two sharp peaks at ∼406.4 and ∼757.4 nm and two broad peaks at ∼440 and ∼470 nm. This tail part is still distinguishable in the spectrum of $I_{FEFD,N,dir}$ corresponding to the PL emission excited by the FEFD configuration. Hence, it is essential to split $PL_{FEFD}(\lambda)$ from $I_{FEFD,N,dir}$. Later, we will show that $PL_{FEFD}(\lambda)$ can be recovered by $PL_{FEBD}(\lambda)$. Since $PL_{FEFD}(\lambda)$ and $PL_{FEBD}(\lambda)$ are induced under the same excitation condition with the source beam incidence at the air/f-SiC epilayer interface, the line shapes of these two spectra should be identical. In step 2, the sample holder, which is used for fixing the f-SiC sample, was installed on the sample port, where the line shape of the measured spectrum in this step ($I_{FEFD,N,ind}$) is considered to represent the line shape of the tail part of the excitation beam. Moreover, although $I_{SRC,N}$ also represents the tail part of the excitation beam, the line shapes of $I_{SRC,N}$ and $I_{FEFD,N,ind}$ are slightly different, as shown in the inset (a-ii) of Figure 6. Here, we believe that the line shape of $I_{FEFD,N,ind}$ is more representative of the tail part of the excitation beam enclosed in $I_{FEFD,N,dir}$. In step 3, an f-SiC sample was mounted on the sample holder with the epilayer side facing toward the sample port. For $I_{FEFD,N,dir}$, we have introduced that this spectrum contains $PL_{FEFD}(\lambda)$, which was measured without adding the OD filter. Meanwhile, by recording $I_{FEFD,W,dir}$, which was measured in wide mode with the OD filter, one can obtain the integrated intensity of the attenuated source beam after PL excitation (L_c), as shown in eq 5.

$$L_c = \int_{369nm}^{382nm} I_{FEFD,W}(\lambda)d\lambda \quad (5)$$

In the inset (b-i) of Figure 6, the peak centered at ∼375 nm in the spectrum related to I_{FEBD} is related to the main peak of the excitation beam that has been largely attenuated. In addition, the emergence of another peak centered at ∼404 nm is actually caused by the interband absorption[37] related to f-SiC's entire 6H-SiC-based structure, where the strong absorption of the light with photon energy higher than the band gap of 6H-SiC is expected. For step 4, the related measured spectrum (I_{FEBD}) at the PL-active spectral region, i.e., 450−784 nm, is considered as the PL emission spectrum transmitted through the 6H-SiC substrate, where the transmitted tail part of the excitation beam can be negligible. Here, a three-step process was developed for the extraction of $PL_{FEBD}(\lambda)$. In the first and second steps, I_{FEBD} and the transmittance spectrum of the 6H-SiC substrate (i.e., T_{SUB}) were smoothed by the Savitzky−Golay (SG) filter at the PL-active spectral region, as shown in eqs 6 and 7. Hence, $PL_{FEBD}(\lambda)$, which represents the PL emission spectrum at the interface of f-SiC epilayer/6H-SiC substrate, equals the quotient between the smoothed I_{FEBD} and T_{SUB}, as shown in eq 8. An example of the extraction of $PL_{FEBD}(\lambda)$ is shown in panel (a) of Figure 7. The transmittance

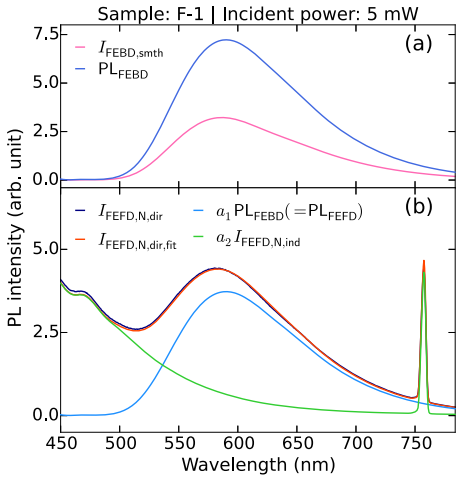

Figure 7. Examples of the PL spectra extraction, here taking sample F-1 at the incident power of 5 mW for example. (a) Extraction of $PL_{FEBD}(\lambda)$ based on eqs 6−8. (b) Extraction of $PL_{FEFD}(\lambda)$ based on eqs 9 and 10.

spectra of the 6H-SiC substrate (SiCrystal, GmbH) of the three f-SiC samples F-1 and F-2/3 employed in this PL-QY determination experiment were measured. Note that the same integrating sphere was applied for the related transmittance measurements with an xenon lamp (HPX-2000, Ocean Optics, Inc.). The raw and smooth transmittance spectra of the 6H-SiC substrate of F-1 and F-2/3 are shown in Figure 8.

$$I_{FEBD}(\lambda)\,|_{450-784nm} \longrightarrow \boxed{\text{SG filter}} \longrightarrow I_{FEBD,smth}(\lambda)\,|_{450-784nm} \quad (6)$$

$$T_{SUB}(\lambda)\,|_{450-784nm} \longrightarrow \boxed{\text{SG filter}} \longrightarrow T_{SUB,smth}(\lambda)\,|_{450-784nm} \quad (7)$$

$$PL_{FEBD}(\lambda) = \frac{I_{FEBD,smth}(\lambda)|_{450-784nm}}{T_{SUB,smth}(\lambda)|_{450-784nm}} \quad (8)$$

Back to the extraction of $PL_{FEFD}(\lambda)$, we have confirmed that $I_{FEFD,N,dir}$ can be split into PL_{FEFD} and the tail part of the incident excitation spectrum. For $PL_{FEFD}(\lambda)$, it has been suggested that $PL_{FEFD}(\lambda) \propto PL_{FEBD}(\lambda)$ since these two spectra have the same excitation condition. However, $I_{FEFD,N,ind}$

DOI: 10.1021/acsomega.9b01753
ACS Omega 2019, 4, 15488−15495

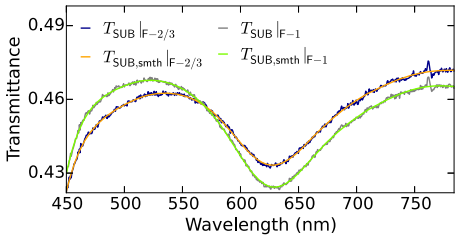

Figure 8. Raw and smooth transmittance spectra of the 6H-SiC substrate of sample F-1 and F-2/3.

representing the line shape of the tail part of the excitation spectrum at FEFD mode has been measured in step 2. Therefore, we got the analytical expression of $I_{FEFD,N,dir}$ at the PL-active spectral region, which corresponds to the linear recombination of $PL_{FEBD}(\lambda)$ and $I_{FEFD,N,ind}$ as shown in eq 9. By solving eq 9 using least-squares regression, one can get $PL_{FEFD}(\lambda)$ via eq 10. An example of the extraction of $PL_{FEFD}(\lambda)$ is shown in panel (c) of Figure 7.

$$\begin{pmatrix} PL_{FEBD}(\lambda) & I_{FEFD,N,ind}(\lambda)|_{450-784nm} \end{pmatrix} \begin{pmatrix} a_1 \\ a_2 \end{pmatrix} = I_{FEFD,N,dir}(\lambda)|_{450-784nm} \tag{9}$$

$$PL_{FEFD}(\lambda) = a_1 PL_{FEBD}(\lambda) \tag{10}$$

4.1.3. Relative Uncertainty. Accordingly, in this research, we can see that P_c is composed of two components that correspond to the PL excitation under FEFD and FEBD modes. The expression of the relative uncertainty of PL-QY (i.e., η_{PL}) has to be considered by following the law of propagating uncertainty,[38] where the expression of η_{PL} refers to eq 11. In eq 11, U_{FEBD}, U_{FEFD}, U_{L_a}, U_{L_c}, and U_{SCR} refer to the relative uncertainties of $P_{c,FEBD}$, $P_{c,FEFD}$, L_a, L_c, and SCR, respectively. In addition, $\sigma_x|_{x\,=\,FEBD,FEFD,L_a,L_c,SCR}$ corresponds to the standard deviations of each variable shown in eq 11, and the expressions included in the angle brackets are related to the respective mean values.

$$\begin{aligned} U_{PL} &= (U_{FEBD}^2 + U_{FEFD}^2 + U_{L_a}^2 + U_{L_c}^2 + U_{SCR}^2)^{0.5} \\ &= \left[\left(\left\langle \frac{P_{c,FEBD}}{P_{c,FEBD} + P_{c,FEFD} + P_{c,BEFD}} \right\rangle \times \frac{\sigma_{FEBD}}{\langle P_{c,FEBD} \rangle} \right)^2 \right. \\ &\quad + \left(\left\langle \frac{P_{c,FEFD}}{P_{c,FEBD} + P_{c,FEFD} + P_{c,BEFD}} \right\rangle \times \frac{\sigma_{FEFD}}{\langle P_{c,FEFD} \rangle} \right)^2 \\ &\quad + \left(\left\langle \frac{L_a}{L_a - L_c} \right\rangle \times \frac{\sigma_{L_a}}{\langle L_a \rangle} \right)^2 + \left(\left\langle \frac{L_c}{L_a - L_c} \right\rangle \times \frac{\sigma_{L_c}}{\langle L_c \rangle} \right)^2 \\ &\quad \left. + \left(\frac{\sigma_{SCR}}{\langle SCR \rangle} \right)^2 \right]^{0.5} \end{aligned} \tag{11}$$

4.2. TRPL Measurement. In this research, the TRPL measurements on f-SiC samples are realized by the time-correlated single-photon counting (TCSPC) system from PicoQuant GmbH. The key components of the TCSPC system are (a) a picosecond laser diode head (LDH-D-C-375) with λ of 375 nm and FWHM of ~44 ps; (b) a computer-controlled diode laser driver (PDL 828 "Sepia II", two channel version); (c) a hybrid photomultiplier detector assembly (PMA Hybrid 40); and (d) a TCSPC board (TimeHarp 260 PICO) with a digital resolution of around 25 ps. Both the injected laser pulse and the emitted photon signal are fiber-coupled to a 50× microscope lens with the configuration of front excitation−front detection. After excitation, the emitted photons are filtered by a 405 nm long-pass filter and then transferred to a photomultiplier tube. A 2 ms time span for photon decay sampling, a 500 Hz repetition rate of laser pulse (i.e., 80 ns resolution), a 1 h integration time were chosen for the TRPL measurement.

AUTHOR INFORMATION

Corresponding Author

*E-mail: haou@fotonik.dtu.dk.

ORCID

Haiyan Ou: 0000-0002-0538-8230

Notes

The authors declare no competing financial interest.

ACKNOWLEDGMENTS

The authors would like to thank Assoc. Prof. Mikael Syväjärvi and Dr. Valdas Jokubavicius from IFM, Linköping University for growing 6H f-SiC samples for this research. This study was supported by Innovation Fund Denmark (No. 4106-00018B).

REFERENCES

(1) Narukawa, Y.; Niki, I.; Izuno, K.; Yamada, M.; Murazaki, Y.; Mukai, T. Phosphor-Conversion White Light Emitting Diode Using InGaN Near-Ultraviolet Chip. *Jpn. J. Appl. Phys.* **2002**, *41*, L371.

(2) Kamiyama, S.; et al. Extremely high quantum efficiency of donor-acceptor-pair emission in N- and B-doped 6H-SiC. *J. Appl. Phys.* **2006**, *99*, No. 093108.

(3) Kamiyama, S.; Iwaya, M.; Takeuchi, T.; Akasaki, I.; Syväjärvi, M.; Yakimova, R. Fluorescent SiC and its application to white light-emitting diodes. *J. Semicond.* **2011**, *32*, No. 013004.

(4) Kamiyama, S.; Iwaya, M.; Takeuchi, T.; Akasaki, I.; Yakimova, R.; Syväjärvi, M. White light-emitting diode based on fluorescent SiC. *Thin Solid Films* **2012**, *522*, 23−25.

(5) Ou, H.; Ou, Y.; Argyraki, A.; Schimmel, S.; Kaiser, M.; Wellmann, P.; Linnarsson, M. K.; Jokubavicius, V.; Sun, J.; Liljedahl, R.; Syväjärvi, M. Advances in wide bandgap SiC for optoelectronics. *Eur. Phys. J. B* **2014**, *87*, 58.

(6) Syväjärvi, M.; Yakimova, R. In *Comprehensive Semiconductor Science and Technology*; Bhattacharya, P., Fornari, R., Kamimura, H., Eds.; Elsevier: Amsterdam, 2011; pp 202−231.

(7) Jokubavicius, V.; Hens, P.; Liljedahl, R.; Sun, J. W.; Kaiser, M.; Wellmann, P.; Sano, S.; Yakimova, R.; Kamiyama, S.; Syväjärvi, M. Effects of source material on epitaxial growth of fluorescent SiC. *Thin Solid Films* **2012**, *522*, 7−10.

(8) Wellmann, P. J. Review of SiC crystal growth technology. *Semicond. Sci. Technol.* **2018**, *33*, No. 103001.

(9) Syväjärvi, M.; Yakimova, R.; Jacobsson, H.; Janzén, E. Structural improvement in sublimation epitaxy of 4H-SiC. *J. Appl. Phys.* **2000**, *88*, 1407−1411.

(10) Wellmann, P.; Desperrier, P.; Müller, R.; Straubinger, T.; Winnacker, A.; Baillet, F.; Blanquet, E.; Marc Dedulle, J.; Pons, M. SiC single crystal growth by a modified physical vapor transport technique. *J. Cryst. Growth* **2005**, *275*, e555−e560.

(11) Sakwe, S. A.; Stockmeier, M.; Hens, P.; Müller, R.; Queren, D.; Kunecke, U.; Konias, K.; Hock, R.; Mager, A.; Pons, M.; Winnacker, A.; Wellmann, P. Bulk growth of SiC - Review on advances of SiC vapor growth for improved doping and systematic study on dislocation evolution. *Phys. Status Solidi B* **2008**, *245*, 1239−1256.

(12) Wei, Y.; Tarekegne, A. T.; Ou, H. Double D-centers related donor-acceptor-pairs emission in fluorescent silicon carbide. *Opt. Mater. Express* **2019**, *9*, 295−303.

(13) Würth, C.; Grabolle, M.; Pauli, J.; Spieles, M.; Resch-Genger, U. Relative and absolute determination of fluorescence quantum yields of transparent samples. *Nat. Protoc.* **2013**, *8*, 1535−1550.

DOI: 10.1021/acsomega.9b01753
ACS Omega 2019, 4, 15488−15495

(14) de Mello, J. C.; Wittmann, H. F.; Friend, R. H. An improved experimental determination of external photoluminescence quantum efficiency. *Adv. Mater.* **1997**, *9*, 230−232.
(15) Braun, D.; Staring, E.; Demandt, R.; Rikken, G.; Kessener, Y.; Venhuizen, A. Photo- and electroluminescence efficiency in poly-(dialkoxy-p-phenylenevinylene). *Synth. Met.* **1994**, *66*, 75−79.
(16) Greenham, N.; Samuel, I.; Hayes, G.; Phillips, R.; Kessener, Y.; Moratti, S.; Holmes, A.; Friend, R. Measurement of absolute photoluminescence quantum efficiencies in conjugated polymers. *Chem. Phys. Lett.* **1995**, *241*, 89−96.
(17) Pålsson, L.-O.; Monkman, A. P. Measurements of Solid-State Photoluminescence Quantum Yields of Films Using a Fluorimeter Measurements of Solid-State Photoluminescence Quantum Yields of Films Using a Fluorimeter. *Adv. Mater.* **2002**, *14*, 757−758.
(18) Johnson, A. R.; Lee, S.-J.; Klein, J.; Kanicki, J. Absolute photoluminescence quantum efficiency measurement of light-emitting thin films. *Rev. Sci. Instrum.* **2007**, *78*, No. 096101.
(19) Murase, N.; Li, C. Consistent determination of photo-luminescence quantum efficiency for phosphors in the form of solution, plate, thin film, and powder. *J. Lumin.* **2008**, *128*, 1896−1903.
(20) Leyre, S.; Coutino-Gonzalez, E.; Joos, J. J.; Ryckaert, J.; Meuret, Y.; Poelman, D.; Smet, P. F.; Durinck, G.; Hofkens, J.; Deconinck, G.; Hanselaer, P. Absolute determination of photoluminescence quantum efficiency using an integrating sphere setup. *Rev. Sci. Instrum.* **2014**, *85*, No. 123115.
(21) Porrès, L.; Holland, A.; Pålsson, L.-O.; Monkman, A. P.; Kemp, C.; Beeby, A. Absolute Measurements of Photoluminescence Quantum Yields of Solutions Using an Integrating Sphere. *J. Fluoresc.* **2006**, *16*, 267−273.
(22) Ishida, H.; Tobita, S.; Hasegawa, Y.; Katoh, R.; Nozaki, K. Recent advances in instrumentation for absolute emission quantum yield measurements. *Coord. Chem. Rev.* **2010**, *254*, 2449−2458.
(23) Würth, C.; Lochmann, C.; Spieles, M.; Pauli, J.; Hoffmann, K.; Schüttrigkeit, T.; Franzl, T.; Resch-Genger, U. T. Evaluation of a commercial integrating sphere setup for the determination of absolute photoluminescence quantum yields of dilute dye solutions. *Appl. Spectrosc.* **2010**, *64*, 733−741.
(24) Wei, Y.; Tarekegne, A. T.; Ou, H. Influence of negative- U centers related carrier dynamics on donor-acceptor-pair emission in fluorescent SiC. *J. Appl. Phys.* **2018**, *124*, No. 054901.
(25) Sridhara, S.; Eperjesi, T.; Devaty, R.; Choyke, W. Penetration depths in the ultraviolet for 4H, 6H and 3C silicon carbide at seven common laser pumping wavelengths. *Mater. Sci. Eng., B* **1999**, *61-62*, 229−233.
(26) Klein, P. B. Carrier lifetime measurement in n- 4H-SiC epilayers. *J. Appl. Phys.* **2008**, *103*, No. 033702.
(27) Kim, J.-S.; Ho, P. K. H.; Greenham, N. C.; Friend, R. H. Electroluminescence emission pattern of organic light-emitting diodes: Implications for device efficiency calculations. *J. Appl. Phys.* **2000**, *88*, 1073−1081.
(28) Wei, Y. Characterization and Simulation of Fluorescent Silicon Carbide: A Study of Donor-Acceptor-Pairs and Intrinsic Defects. Ph.D. thesis,Technical University of Denmark: 2019.
(29) Hayashi, T.; Asano, K.; Suda, J.; Kimoto, T. Impacts of reduction of deep levels and surface passivation on carrier lifetimes in p -type 4H-SiC epilayers. *J. Appl. Phys.* **2011**, *109*, No. 114502.
(30) Galeckas, A.; Grivickas, V.; Linnros, J.; Bleichner, H.; Hallin, C. Free carrier absorption and lifetime mapping in 4H SiC epilayers. *J. Appl. Phys.* **1997**, *81*, 3522−3525.
(31) Takeshima, M. Effect of Auger recombination on laser operation in GaAlAs. *J. Appl. Phys.* **1985**, *58*, 3846−3850.
(32) Galeckas, A.; Linnros, J.; Grivickas, V.; Lindefelt, U.; Hallin, C. Auger recombination in 4H-SiC: Unusual temperature behavior. *Appl. Phys. Lett.* **1997**, *71*, 3269.
(33) Ščajev, P.; Gudelis, V.; Jarašiūnas, K.; Klein, P. B. Fast and slow carrier recombination transients in highly excited 4H- and 3C-SiC crystals at room temperature. *J. Appl. Phys.* **2010**, *108*, No. 023705.
(34) Ščajev, P.; Jarašiunas, K. Temperature- and excitation-dependent carrier diffusivity and recombination rate in 4H-SiC. *J. Phys. D: Appl. Phys.* **2013**, *46*, No. 265304.
(35) Ščajev, P. Application of excite-probe techniques for determination of surface, bulk and nonlinear recombination rates in cubic SiC. *Mater. Sci. Eng. B* **2014**, *185*, 37−44.
(36) Aad, R.; Divay, L.; Bruyant, A.; Blaize, S.; Couteau, C.; Rogers, D. J.; Lerondel, G. Leaky mode analysis of luminescent thin films: The case of ZnO on sapphire. *J. Appl. Phys.* **2012**, *112*, No. 063112.
(37) Choyke, W. In *Silicon Carbide-1968*; Henisch, H., Roy, R., Eds.; Elsevier, 1969; pp S141−S152.
(38) ISO, I.; OIML, B. Guide to the Expression of Uncertainty in Measurement. Geneva, Switzerland, 1995,

DOI: 10.1021/acsomega.9b01753
ACS Omega 2019, 4, 15488−15495